Mesoscale and diel to monthly variability of CO_2 and carbon fluxes at the ocean surface in the northeastern Atlantic

Liliane Merlivat,[1] Melchor Gonzalez Davila,[2] Guy Caniaux,[3] Jacqueline Boutin,[1] and Gilles Reverdin[1]

Received 22 November 2007; revised 4 September 2008; accepted 9 January 2009; published 17 March 2009.

[1] Four CARIOCA Lagrangian buoys were deployed in the northeast Atlantic Ocean as part of the Programme Océan Multidisciplinaire Méso Echelle (POMME) dedicated to the study of the role of mesoscale eddies in biological production, the carbon budget, and the subduction of mode waters. An extensive set of hourly surface measurements of temperature, salinity, and carbon dioxide fugacity (fCO_2) was collected from February to August 2001. The high-frequency spatial and temporal variability observed in surface fCO_2 and in the derived dissolved inorganic carbon (DIC) concentrations suggests that abrupt changes of the carbon variables are being generated along frontal patterns and filaments by submesoscale and mesoscale eddy-eddy interactions, especially in winter. On the basis of a 1-D model of the diurnal mixed layer along the buoy trajectory, we show that under certain conditions the diel cycle of DIC is driven by the daily cycle of photosynthesis and metabolic CO_2 release at the ocean surface. This information is quantitatively used to derive in-situ primary production, carbon gross, and net community production. The analysis of 107 observed diel cycles of DIC shows that episodic biological production processes are triggered by the mesoscale activity of surface eddies. Over the sampled period, the POMME area is a sink for atmospheric CO_2 with an estimated flux of -4 mmol m^{-2} day^{-1}. The calculated amount of anthropogenic carbon transported into the ocean interior by subduction of subpolar mode water is equal to 2.8 10^{13} gC yr^{-1}.

Citation: Merlivat, L., M. Gonzalez Davila, G. Caniaux, J. Boutin, and G. Reverdin (2009), Mesoscale and diel to monthly variability of CO_2 and carbon fluxes at the ocean surface in the northeastern Atlantic, *J. Geophys. Res.*, *114*, C03010, doi:10.1029/2007JC004657.

1. Introduction

[2] In 2001, the French Programme Océan Multidisciplinaire Méso Echelle (POMME) carried out a coordinated multidisciplinary field experiment to investigate the subduction mechanisms of subpolar mode water in the northeast Atlantic and how this affects the carbon budget and the biological production [*Mémery et al.*, 2005]. These issues are crucial for improving our understanding of the oceanic carbon cycle since this area is both a strong sink of atmospheric CO_2 [*Gonzalez Davila et al.*, 2005; *Sabine et al.*, 2004] as well as a region where the subducted surface waters transport anthropogenic carbon into the deep water, where they are isolated from the atmosphere on decadal timescales. Moreover, subduction and the beginning of the spring bloom occur at approximately the same time at the end of winter when the mixed layer shoals, and thus the respective timing of the bloom and subduction processes largely controls the biogeochemical properties of the water masses that are further subducted into the main thermocline. POMME was also conducted with a strong emphasis on the dynamics of mesoscale eddies.

[3] The POMME experiment was carried out in a region of the northeast Atlantic Ocean between 38°N and 45°N and 16°W and 21°W. In this region, located between the subpolar and the subtropical gyre; the maximum winter mixed layer depth is 300 m, with mixed layer depths generally being deeper in the north than in the south of the area. Three field studies were conducted over three seasons in 2001 to study conditions during the prebloom period (the winter cruise, 3 February to 19 March), the bloom period (the spring cruise, 24 March to 3 May), and the postbloom period (the summer cruise, 26 August to 8 October). Each cruise was divided into two legs. Physical and biogeochemical measurements, including the inorganic carbon system variables, were made during the first leg of each of the three cruises.

[4] Four carbon interface ocean atmosphere (CARIOCA) Lagrangian drifters were deployed during the first leg of the

[1] Laboratoire d'Océanographie et du Climat-Expérimentation et Approches Numériques (ex LODYC)/IPSL, Centre National de la Recherche Scientifique, Université Pierre et Marie Curie, Paris, France.
[2] Facultad de Ciencias del Mar, Universidad de Las Palmas de Gran Canaria, Las Palmas, Spain.
[3] Centre National de Recherches Meteorologiques/GAME (Météo-France/CNRS), Toulouse, France.

0148-0227/09/2007JC004657

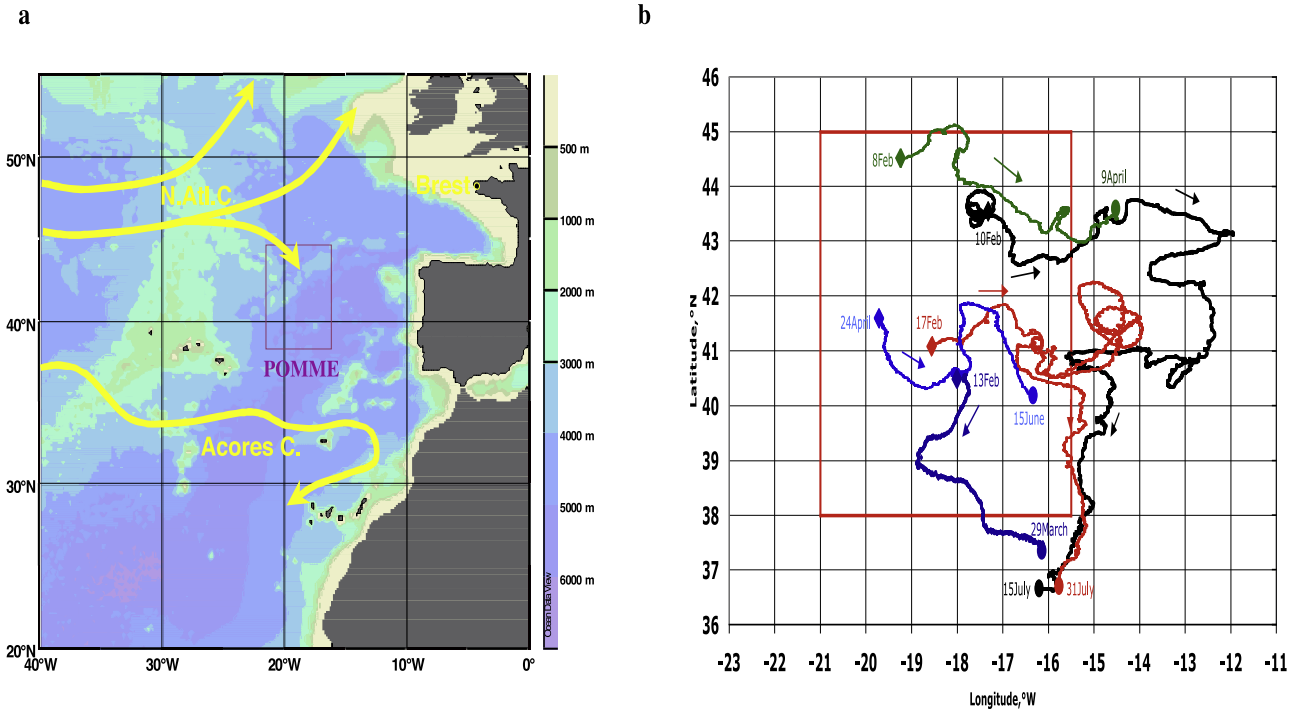

Figure 1. (a) Map of the Programme Océan Multidisciplinaire Méso Echelle (POMME) area. Bathymetry is represented by shaded colored contours. The yellow arrows indicate the location of the North Atlantic and Azores currents. The red square is the area of intensive in-situ survey during the POMME program in 2001. (b) Chart showing the area in which the buoys were drifting between February and August 2001. The color code for the buoys is as follows: red P1, blue for P2, light for P2b, green for P3, and black for P4. The location of the deployment of each buoy is indicated by a diamond. Ellipses indicate the end point of the trajectories along which measurements of fCO_2 and DIC were taken. The arrows show the mean components of the direction of motion of the buoys mainly eastward and southward. The purple square is identical to the red one shown on Figure 1a.

winter cruise. The purpose of this paper is to interpret the temporal and spatial variability of the fugacity of carbon dioxide (fCO_2) measured at the ocean surface by these four buoys and the derived total dissolved inorganic carbon concentration (DIC).

[5] This paper is organized as follows: in section 2, Data and Methods, we describe the parameters measured or computed from the buoy data as well as measurements of the carbon system parameters, fCO_2 and DIC, and other in-situ parameters made from the ship when the four drifters were launched. We also present a 1-D model of the upper mixed layer used to simulate mixed layer properties along the buoy trajectory. In section 3, an overview of the full set of fCO_2 and DIC measured by the four drifters is given. We analyze the role of mesoscale circulation on the distribution of fCO_2 and DIC at the ocean surface in winter conditions. The variability of observed diurnal in-situ DIC is then investigated in order to quantify the daily carbon gross and net community production measured in-situ close to the sea surface. These estimates are compared with results of measurements based on in vitro incubation techniques. Finally, an attempt is made to quantify the efficiency of the biological pump for sequestering inorganic carbon in the upper mixed layer of the POMME area over the three months period from March to June. In section 4, buoy data are combined with satellite measurements of wind speed and sea surface temperature (SST) to compute the air-sea CO_2 flux over the six months period extending from February to August 2001. We then derive an estimate of the amount of atmospheric anthropogenic carbon that has been subducted in deep water in late winter in the northern part of the POMME area. Summary and conclusions are the subject of section 5.

2. Data and Methods

2.1. Investigation Zone and Sampling Strategy

[6] The area investigated is a rectangle, 500-km longitude by 750-km latitude, centered at 41.5°N, 19°W between the Iberian Peninsula and the Azores Archipelago (Figure 1a). It encompasses the so-called discontinuity zone, which corresponds to a transition zone between two main areas: the northern part is characterized by a deep late winter mixed layer (up to 300 m), while shallow (100–150 m) winter mixed layers are observed in the southern part. Subduction in this area has been investigated and explained in terms of advection of subpolar mode water to the south by the southern branches of the North Atlantic current across the steep mixed layer depth gradient [*Paillet and Arhan*, 1996]. At the basin scale, these hydrological differences have potential implications for the timing as well as on the intensity of the spring bloom. In addition, this part of the

Table 1. Summary of the Deployment Conditions of the Four Buoys During the February Winter Cruise[a]

Date Station	Buoy	Lat. °N	Long. °W	fCO_2 Ship/ *fCO_2 Buoy* (μatm)	DIC Ship/ *DIC Buoy* (μmol kg^{-1})	fCO_2 Buoy − fCO_2 Ship (μatm)	DIC Buoy − DIC Ship (μmol kg^{-1})
8 Feb. station 16	P3	44°49	19°31	352.9	2108.5	−1.9	−1.8
				351.0	*2106.7*		
10 Feb. station 23	P4	43°53	17°35	347.1	2106.2	+1.6	−0.3
				348.7	*2105.9*		
13 Feb. station 35	P2	40°50	18°00	338.9	2096.8	+0.9	−2.8
				339.8	*2094.0*		
17 Feb. station 52	P1	41°00	18°67	334.7	2092.3	+0.3	+2.5
				335.0	*2094.8*		

[a]Comparison between the values of fCO_2 and DIC measured on the ship (underway for fCO_2 and at hydrological station for DIC) and by the buoys.

northeast Atlantic is subjected to significant mesoscale activity (current meandering, presence of eddies), which is expected to impact both the magnitude and the location of primary productivity.

[7] Within the POMME study area, and with the objective of covering the three main hydrological and biogeochemical bloom conditions, the sampling strategy was based on three ~55 day cruises in 2001. Each cruise was divided into two legs. The first legs were devoted to a quasi-synoptic survey of the area. They consisted of a network of ~80 conductivity-temperature-depth (CTD) rosette stations down to a depth of 2000 m (spaced by 30 nautical miles) for the measurement of core hydrological and biogeochemical properties, including the inorganic carbon system variables. Continuous underway fCO_2 measurements in the surface seawater were also performed [*González Dávila et al.*, 2005]. The second legs were focused on process studies at four stations. A synoptic survey associated with quasi real-time data assimilation and modeling was conducted to resolve the range of variability in mesoscale structures (fronts, eddies, meanders, gyres) typical of this area [*Paci et al.*, 2005].

[8] During the first leg of the winter cruise (3 to 24 February), four CARIOCA drifters (referred to hereafter as P1, P2, P3, and P4) were deployed after the completion of a CTD rosette station. One of them, P2, was recovered on 29 March during the first leg of the spring cruise as it was leaving the POMME study area, and was then redeployed on 24 April 24 in the central part of the zone during the second leg of the spring cruise (P2b). The trajectories followed by the buoys between February and August indicate an eastward and southward prevailing drift motion (Figure 1b). Compared to the core study area of the POMME program, the range of latitude covered by the buoys is similar but the area sampled by the buoys extends further east.

2.2. CARIOCA Buoys

[9] Hourly measurements made by the buoys are: wind speed and barometric pressure at a height of 2 m above the sea surface, and water-side measurements of sea surface temperature (SST), salinity (SSS), fCO_2, and fluorescence at a depth of 2 m [*Merlivat and Brault*, 1995; *Hood and Merlivat*, 2001; *Bakker et al.*, 2001; *Copin-Montegut et al.*, 2004]. SSS is measured using Microcat SBE 37-SI sensors. Finally, each buoy is equipped with a drogue anchored at a mean depth of 15 m in order to constrain its trajectory to follow the upper ocean surface circulation. Data are transmitted in near real time by Argos telemetry.

[10] Hourly measurements of SST, SSS and fCO_2 are used to compute time series of DIC using the carbonic acid dissociation constants of *Lueker et al.* [2000] and the linear relationship established from measurements of discrete surface alkalinity samples (<10 m) and salinity during the three cruises of the POMME program [*González Dávila et al.*, 2005], where

$$A_T = 107.5 + 62.59^* \text{ S } \left(r^2 = 0.92, n = 212\right)'$$

with a standard error ±2.25 μmol kg^{-1}.

[11] Buoys and ship-based measurements are compared at the buoy deployment site. The ship fCO_2 data were obtained from the continuous underway measurement system, while ship DIC is calculated from the water samples taken at a depth between 5 and 10 m during the CTD cast (http://www.lodyc.jussieu.fr/POMME/site_data_bateau_frame.html). There is a delay of a few hours between the measurements made by the buoy and those made on board the ship, because the ship leaves the station just after the buoy has been deployed, and the time for stabilization of the buoy fCO_2 sensor after deployment is approximately six hours. The differences between both sets of data are smaller than 2 μatm for fCO_2 and 3 μmol kg^{-1} for DIC (Table 1). These differences are roughly similar to the limits of the accuracy of the different types of instruments as well as the natural time and space variability of the values of fCO_2 and DIC in seawater.

[12] The value of the partial pressure of atmospheric CO_2, pCO_{2atm}, is computed as

$$pCO_{2atm} = x\ (P - pH_2O)$$

where P in atmosphere is the atmospheric pressure measured by the buoys, pH_2O is the saturation partial pressure of water vapor, in atmosphere, at the SST measured by the buoys. x is the molar fraction of CO_2 in dry air in ppm (10^{-6}). We use monthly atmospheric xCO_2 provided by Globalview-CO_2 (2001, available via anonymous FTP at ftp.cmdl.noaa.gov,path:ccg/co2/GLOBALVIEW) at Terceira Island, Azores, Portugal (38.77°N−27.38°W). We consider these values representative of the atmospheric xCO_2 mean values over the POMME area, as they agree with the measurements made on board the ship during the

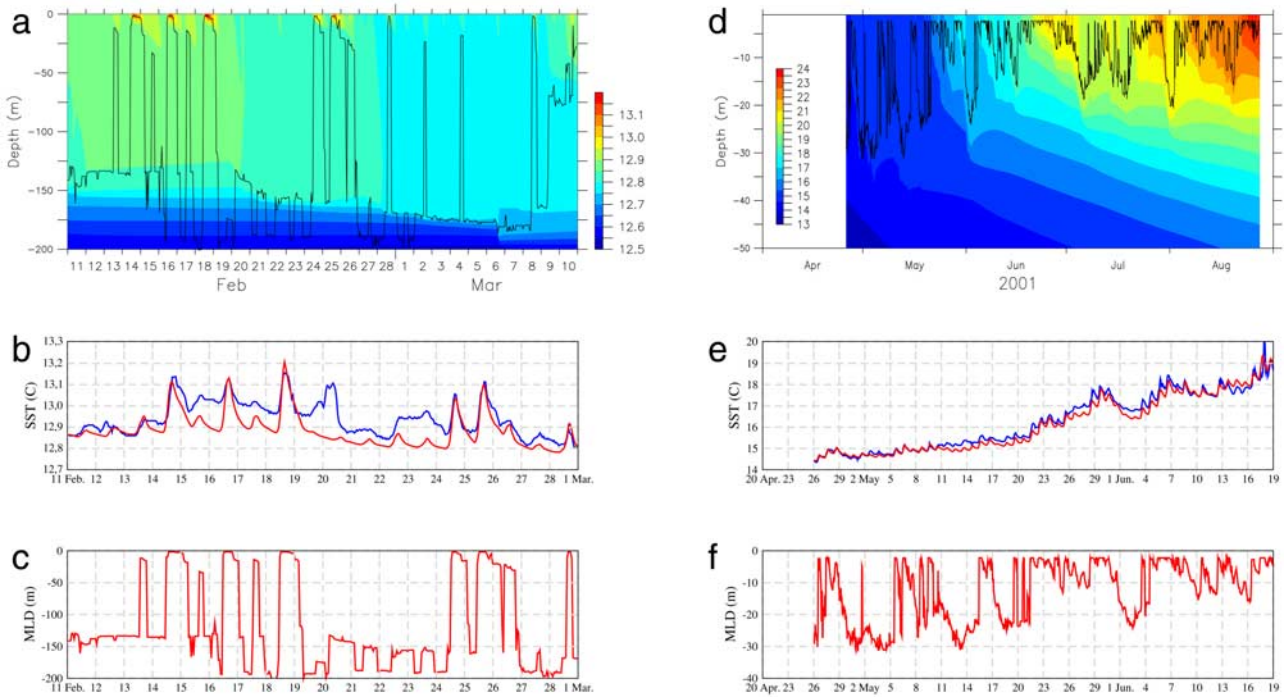

Figure 2. (a) Model MLD and temperature distribution in the upper 200 m along the trajectory of the P4 buoy from 11 February to 10 March. (b) Time variation of SST measured by the buoy from 11 February to 1 March (blue); model SST (red). (c) Model MLD. (d) Same as Figure 2a for P2b buoy in the upper 50 m from 26 April to 31 August 31. (e, f) Same as Figures 2b and 2c for P2b buoy from 26 April to 19 June.

winter and spring cruises. The fugacity fCO_{2atm} is computed from pCO_{2atm} [*Zeebe and Wolf-Gladrow*, 2001].

[13] The CO_2 flux, F_{CO2}, at the air-sea interface is equal to

$$F_{CO_2} = k\alpha(\Delta fCO_2)_{sea-air}$$
$$F_{CO_2} = K(\Delta fCO_2)_{sea-air} \quad (1)$$

where k is the CO_2 gas transfer velocity, α is the solubility of CO_2 in sea water [*Weiss*, 1974], K = kα, the gas exchange coefficient and $(\Delta fCO_2)_{sea-air}$, the sea-air fCO_2 difference. The value of the gas transfer velocity is computed according to the short-term k-U relationship of [*Wanninkhof*, 1992]

$$k = 0.31\ U^2 \left(\frac{Sc}{660}\right)^{-0.5} \quad (2)$$

where k is in cm h^{-1}, U, the wind speed U in m s^{-1} and Sc the Schmidt number of CO_2.

2.3. 1-D Modeling of the Mixed Layer Depth (MLD) Along the Buoy Trajectory

[14] A 1-D model was used to estimate the mixed layer depth along the buoy trajectory, which cannot be estimated from the information measured by the buoy itself. Horizontal advection and mixing are assumed to be negligible. The physics of the model combines a simple eddy kinetic energy parameterization of the oceanic vertical mixing [*Gaspar et al.*, 1990] with a diapycnal mixing scheme [*Josse et al.*, 1996]. The vertical resolution of the model is one meter. The time step is 15 minutes. Hourly surface atmospheric and radiative forcing are computed and derived from the work of *Caniaux et al.* [2005a, 2005b], analysis of surface fluxes. These fluxes were produced specifically for the whole POMME area on a fine mesh domain [*Caniaux et al.*, 2005a] and adjusted with a generic genetic algorithm so that the whole area heat budget deduced from observations could be closed [*Caniaux et al.*, 2005b]. Model validation exercises [*Paci et al.*, 2005; *Giordani et al.*, 2005; *Lévy et al.*, 2005] suggest that these fluxes are particularly well suited for obtaining realistic oceanic surface properties and budgets. These gridded fluxes (5-km grid mesh) used hourly available radiative satellite retrievals (solar heat and downwelling infrared radiation) and adjusted turbulent fluxes every six hours. For the present study, these fluxes were interpolated at the location of the buoys, at the time step of the model, a high temporal resolution that reproduced the diurnal cycle. The initial conditions for temperature and salinity profiles are taken from the closest (in time and position when available) CTD cast to the buoys.

[15] A comparison between model SST and temperature and salinity measurements made by the buoy provides an indication of the validity of the numerical simulation. Discrepancies between the hourly values of SST measured by the buoys or computed by the model, for example, on 20 February on Figure 2b, indicate that the surface temperature is no longer uniquely controlled by just the atmospheric fluxes as assumed in the model, but could be the result of a

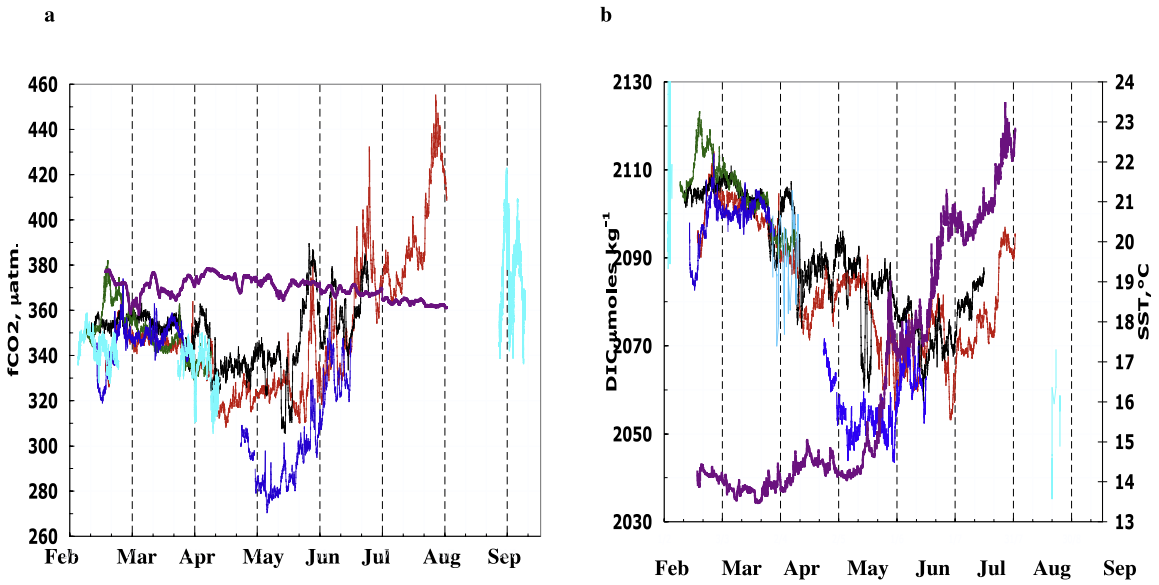

Figure 3. Time variation of (a) fCO_2 and (b) DIC and SST from February to September. The color code used for the buoy data is the same as Figure 1. The measurements made during the hydrological surveys of the R/V *Atalante* are shown in cyan. In Figure 3a the purple line indicates the atmospheric fCO_2 value. In Figure 3b the purple line indicates SST of buoy P1.

change of water mass properties (lateral or vertical mixing) along the trajectory of the buoys.

3. Dynamical and Biological Processes Driving fCO_2 and DIC Surface Variability

3.1. Distribution of fCO_2 and DIC From Winter to Early Summer

[16] Figures 3a and 3b represent the full set of measurements of fCO_2 and calculated values of DIC between February and 1 August along the trajectories followed by the 4 buoys (Figure 1b). The longest time series of carbon data have been obtained for the P1 and P4 buoys; respectively, 164 and 154 days. The other two drifters only provided data for approximately 50 days owing to CO_2 sensor failures. The data acquired on board the ship during the first leg of the three POMME cruises are also indicated.

[17] There are two main features to note in Figure 3. The values of fCO_2 in seawater are mostly lower than the value in the atmosphere from February until the end of June. This indicates that the ocean is a sink for atmospheric CO_2 during this five months period. Starting in July, P1 and P4 buoys indicate that the gas flux is reversed, with fCO_2 in seawater larger than the atmospheric concentration because of seasonal thermal heating.

[18] A marked decrease of DIC from March to June (Figure 3b) is presumably a consequence of the uptake of inorganic carbon by biological processes. In May, a large difference of DIC, close to 35 μmol kg^{-1}, is observed between the data from P2 buoy and P1 and P4 buoys, even though the three buoys were drifting in the same latitudinal range during this time period, 41°N ± 1°N, but seven degrees apart in longitude, between 13°W to 20°W. The trajectory of the P2 buoy was following the front between the cyclonic eddy C4 and the anticyclonic eddies A2 and A4. The two other buoys were drifting in the eastern part of the domain where the front is not clearly distinguishable from the altimeter observations (Figure 4a). Overall, these observations highlight the large spatial heterogeneity of DIC concentrations in zones with frontal eddies, which is certainly the result of the heterogeneity of primary production.

[19] Starting at the beginning of July, two buoys, P1 and P4, drifted southward, out of the POMME latitudinal range (Figure 1b). The observed increase of the DIC values at this period of the year (Figure 3b) is interpreted as a signature of the north–south gradient of DIC clearly identified during the POMME cruise later in August–September, with higher values in the south of the POMME area [*González Dávila et al.*, 2005].

[20] We have looked in detail at the measurements made by the P1 and P4 buoys as they followed similar southward trajectories from 40°N to 37.8°N with a time lag of about ten days. Mean differences of fCO_2 and of DIC are 8.9 μatm. and 4.4 μmol. kg^{-1}, respectively, with the highest values being measured by the P4 buoy, which drifted ahead of the P1 buoy by ten days. Similarly, the mean values of SST and SSS measured by the P4 buoy are higher, 0.12°C and 0.06 in salinity, respectively. These numbers give an indication of the spatial and temporal variability of the ocean surface properties, where the trajectories followed by the buoys are not identical, with longitudinal distances between the buoys of 50 km and measurements made between six and sixteen days apart.

3.2. Surface Mesoscale Signatures During Winter

3.2.1. Comparative Time and Space Sampling by Ships and Buoys

[21] An intense effort has been undertaken in the POMME field study to get an understanding of the upper ocean dynamics, particularly mesoscale activity and mixed layer evolution, during the restratification key period (Winter and Spring from February to May 2001) [*Mémery et al.*,

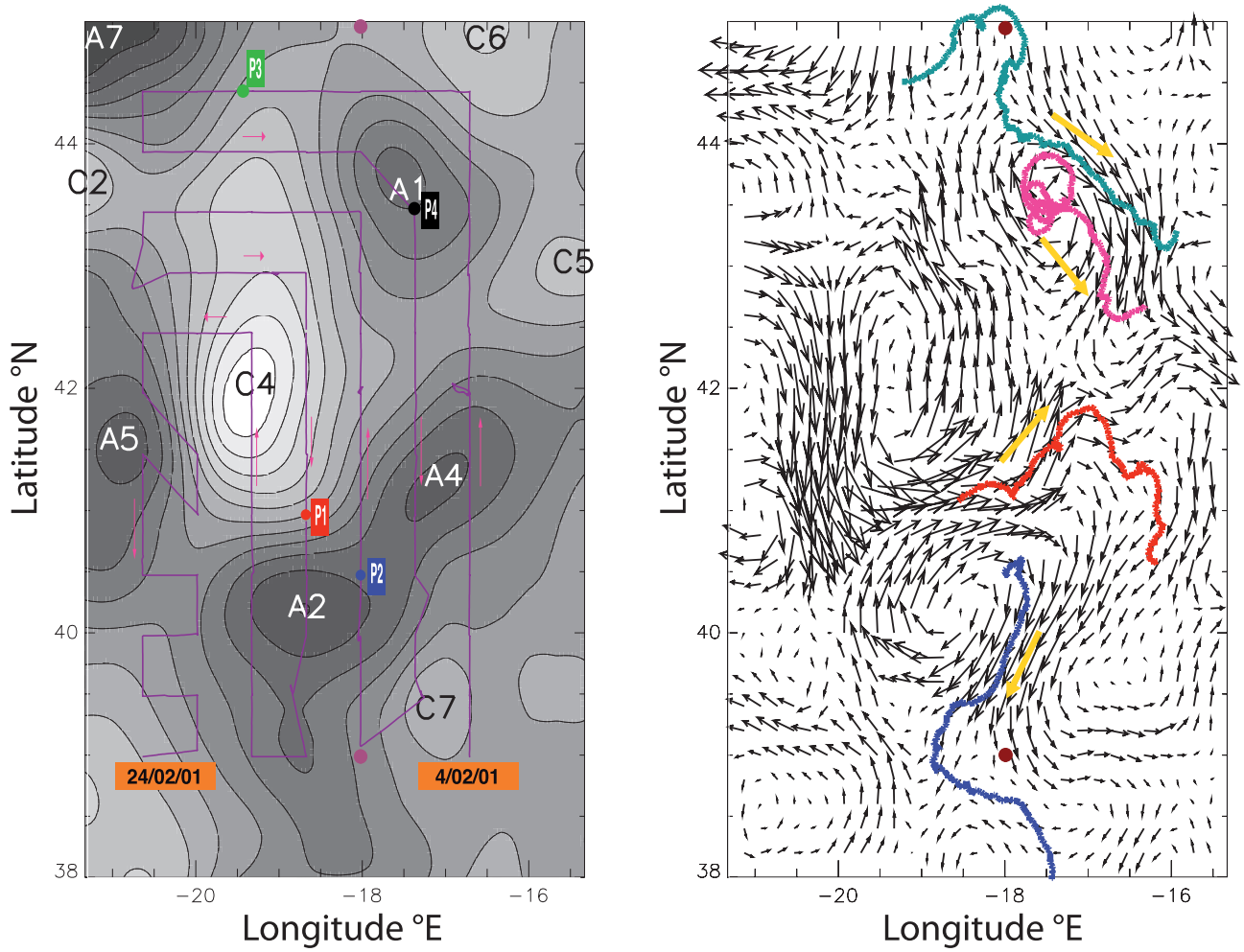

Figure 4. (a) Map of the POMME area. The purple line indicates the route followed by the R/V *Atalante* during the first leg of the winter cruise from 4 February in the southeast corner to 24 February in the southwest corner. The arrows indicate the successive tracks. The sites where the buoys were deployed are indicated by colored squares with the same code as on Figure 1. The contours of SLA around the cyclonic and anticyclonic eddies are indicated in white, grey, and black (white, −10 cm; black, +10 cm). (b) Trajectories of the four buoys superimposed on the currents deduced from geostrophy from the analysis of the hydrographic survey made during the cruise using a reference level of 1700 m [*Paci et al.*, 2005]. The color code is the same as for Figure 1 except for P4 buoy, where for clarity, pink has been used instead of black. Each trajectory indicates the path followed by a buoy up to 15 March. Yellow arrows indicate the mean displacement of the drifters. The brown squares show the location of the moorings anchored at 45°N–18°W and 39°N–18°W.

2005; *Paci et al.*, 2005]. The distribution of sea level anomalies deduced from merged TOPEX/Poseidon and ERS2 altimeters and surface currents deduced from the analysis of the hydrological survey [*Paci et al.*, 2005] is shown on Figures 4a and 4b for the 3 to 24 February cruise period. The presence of cyclonic (C) and anticyclonic (A) mesoscale eddies is clear. The ship track crosses the eddies while the four drifters mainly follow the surface currents around or between the eddies. In order to gain insight into the influence of mesoscale circulation on the surface distribution of inorganic carbon, we analyze the variability of fCO_2 and DIC from both, the ship or the buoy data as a function of latitude (Figures 5a and 5b). The time period considered extends from 3 to 24 February.

[22] The ship data indicate a general north to south decreasing trend of fCO_2 and DIC together with a change of about 20 μatm for fCO_2 and 10 μmol kg^{-1} for DIC in the 40.5°N–41.5°N latitude range between meridional sections from east to west (Figures 5a and 5b). This is associated with the presence of a front located between the anticyclonic eddy A2 and the cyclonic eddy C4 between 18°W and 20°W (Figure 4a), which is not found in the eastern part of the survey. An integrated picture of the surface DIC over the whole POMME area based on the measurements of DIC made at 5-m depth during the February hydrological survey is shown in Figure 4 of *Resplandy et al.* [2009].

[23] The range of variation of fCO_2 and DIC is far larger for the buoy data than observed from the ship, specifically

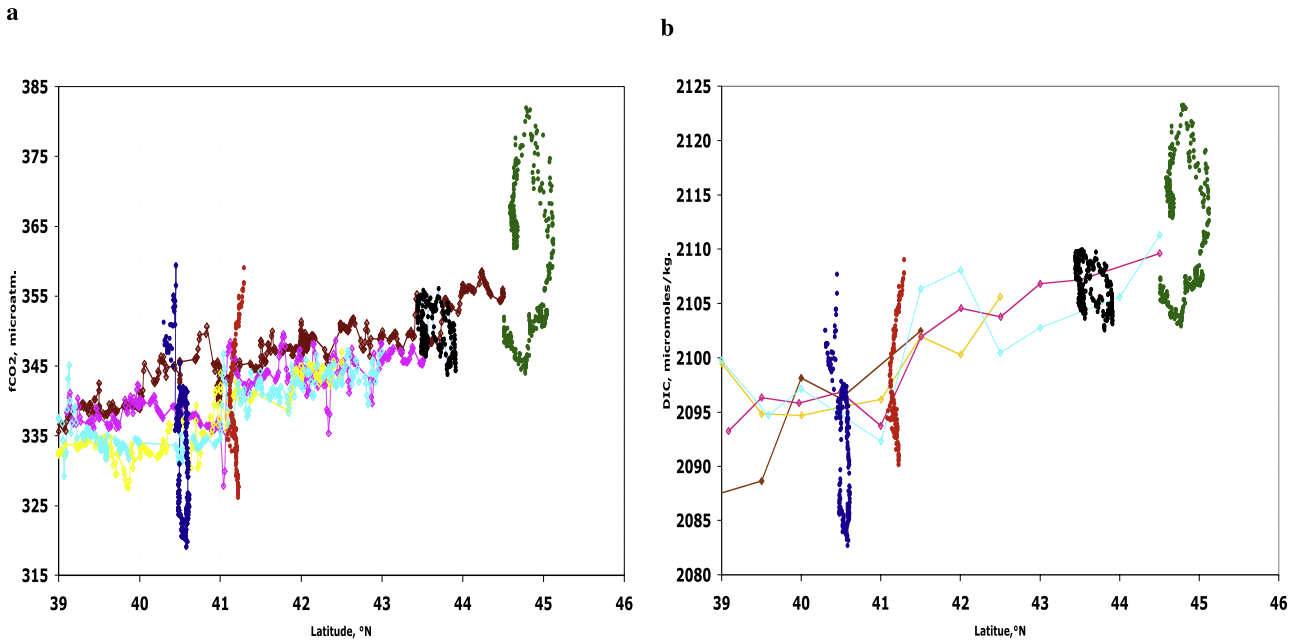

Figure 5. Latitudinal variations of (a) fCO_2 and (b) DIC measured along the north–south tracks of the R/V *Atalante*, shown as colored diamonds at 16.6°W (brown), 18°W (pink), 18.7°W (cyan), and 19.3°W (yellow) from 3 to 24 February and by the four buoys (dots with same color code as in Figure 1) after their deployment until 24 February.

for the P1 and P2 drifters deployed in the vicinity of the front as well as the most northern P3 buoy (Figures 5a and 5b). This is interpreted as the result of high-frequency events affecting the distribution of fCO_2 and DIC at the ocean surface in winter conditions. The situation is different for the P4 drifter. During the time of the ship survey, the trajectory of this drifter followed a clockwise circle 48-km diameter following the inner contour of the anticyclonic eddy A1 (Figure 4a). Over an eleven day period, the mean of the hourly values of fCO_2 and DIC measured by the P4 buoy are, respectively, 349.9 ± 3.1 μatm and 2106.4 ± 1.9 μmol kg^{-1}. For the three other buoys, the standard deviation of the mean values of fCO_2 and DIC are, respectively, 8.8, 9.8 and 10.1 μatm and 5.2, 5.9 and 5.6 μmol kg^{-1}, indicating a much larger variability around the mean value compared to the P4 buoy.

3.2.2. Signature of Deep Mixing in February–March

[24] Figure 6 shows the DIC variability calculated from the measurements made by the four drifters from the time of their deployment until 15 March, i.e., during the period of maximum deepening of the mixed layer, which occurs around the beginning of March in the POMME region [*Paci et al.*, 2005]. The buoys were located in the POMME area, westward of the 16°W longitude. Until 1 March, a very large difference of up to 35 μmol kg^{-1} is observed between the data from the southern buoys compare to the data from the northern buoys, while the total range of variability measured at the surface during the hydrological survey was only 20 μmol kg^{-1}, between 2090 μmol kg^{-1} in the south east of the area and 2110 μmol kg^{-1} in the north (http://www.lodyc.jussieu.fr/POMME/site_data_bateau_frame.html). The variability displayed in the buoy DIC data is mainly caused by mesoscale motions, either lateral or vertical, within the upper surface layer.

[25] We also analyzed the large increase of DIC, up to 2123 μmol kg^{-1}, measured by the P3 buoy, between 15 and 19 February while it was drifting at a mean latitude of 44.8°N and for which we have ancillary data. Temperature and salinity measured at −185 m with a time sampling of one hour were provided by a mooring deployed at 45°N–18°W, at the northern boundary of the region [*Gaillard et al.*, 2005]. Between 15 and 22 February, the P3 buoy drifted at a distance of no more than 25 km from the mooring. For this time interval, we compare the salinity–temperature relationships measured at a depth of 2 m by the buoy with that at 185 m by the mooring (Figure 7). We also provide the CTD salinity-temperature data measured down to the

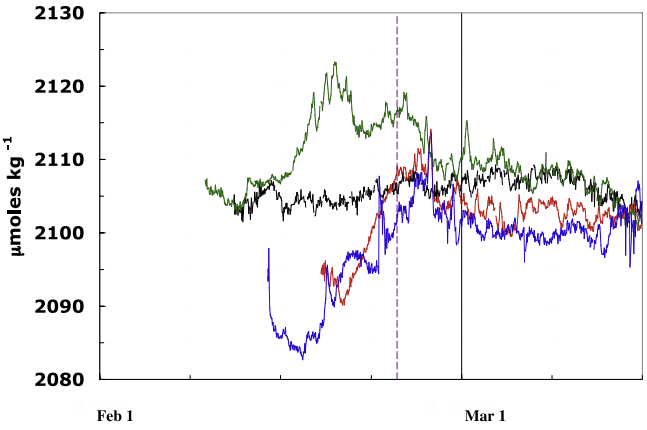

Figure 6. Time evolution of DIC measured by the four buoys after they were launched until 15 March. The dotted purple line indicates the end of the ship survey on 24 February.

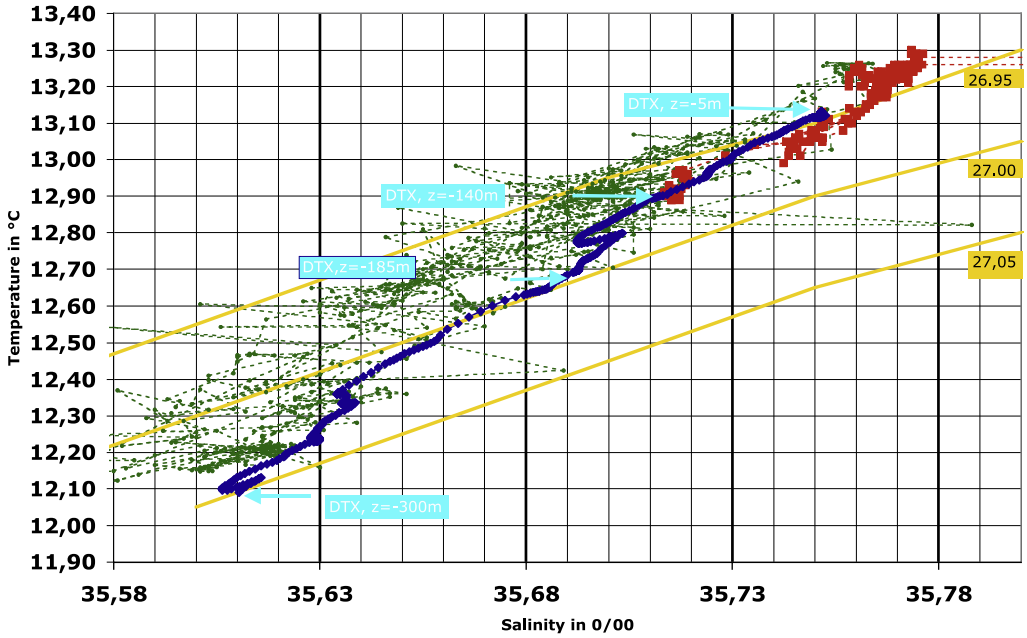

Figure 7. Temperature-salinity relationship measured between 15 and 22 February on the mooring at −185 m (green) and at $z = -2$ m by the P3 buoy (red) at a distance less than 25 km from the mooring. The blue line indicates the data measured from −3 to −300 m during the CTD cast made by the R/V *d'Entrecastraux* on 16 February at the location of the mooring. Yellow lines indicate isodensities.

depth of 300 m close to the mooring on 16 February by the RV *d'Entrecastaux*, a second vessel involved in the POMME program.

[26] As expected, we observe that the ship and mooring data follow the same T-S mixing line. In many cases, the buoy values correspond to this same T-S mixing line, with an extreme point corresponding to a CTD measurement at 140 m, which is a strong indication of a deepening of the MLD to this level induced by short timescale (approximately 3 days) mixing events during winter [*Bouruet-Aubertot et al.*, 2005].

[27] Moreover, the distribution of DIC in the water column was measured from samples collected and analyzed at each CTD cast. DIC increases with depth. Along 18°W, the range of surface concentrations extends from 2094 to 2110 μmol kg^{-1} from 39°N to 44.5°N while it varies from 2135 to 2155 μmol kg^{-1} at a depth of 400 m. At 150 m depth, samples collected at 43°N and 44°N have a density of 26.96 and a DIC equal to 2121 μmol kg^{-1}. These data are very close to the density measured at the surface by the P3 buoy (see Figure 7) as well as the maximum value of DIC equal to 2123 μmol kg^{-1}. This strengthens the assumption of a short-term vertical mixing event (a few days) down to 150 m.

[28] Similarly, between 20 and 25 February, a rapid increase of DIC, close to 4.5 μmol kg^{-1}, is measured by P1 and P2 buoys in the southern part of the area (Figure 6). The DIC profiles from nearby CTD casts, within ±0.5°N, indicate that the maximum value of DIC observed in the surface buoy data, close to 2110 μmol kg^{-1}, is found in a depth range between 60 and 180 m depending on the selected station.

[29] As part of the POMME spring cruise, a high-resolution survey was conducted with a SeaSoar in the upper 330 m of the water column at a location centered around 40.5°N and 19.5°W. Using the SeaSoar data combined with the analysis of altimeter data, *Legal et al.* [2007] showed the development of an energetic vertical velocity field with alternate signs and amplitudes of up to 20 m per day located along filaments between mesoscale eddies. As a consequence, these motions have a significant impact on the profile of a variable such as DIC that already exhibits a strong vertical gradient. The two sets of buoy data discussed above are in close agreement with the conclusions of the work of *Legal et al.* [2007].

[30] In summary, episodic mixing events between the mixed layer and deep water on the timescale of a few days control the large variations seen in surface DIC in late winter.

3.3. Influence of Biology on Surface Carbon Variables at Daily Scale

3.3.1. Estimation of In-Situ Gross and Net Community Production

[31] The 1-D model described previously is reasonably successful in simulating daily stratification in the upper layers. Figure 2 illustrates two situations in which the numerical simulation is validated by the buoy data. Figure 2a (left) shows the time variation of the model mixed layer depth (MLD) and the vertical distribution of the temperature in the upper 200 m of the water column along the trajectory of the P4 buoy during the winter season from 11 February to 10 March. The trajectory of the buoy followed a circle inside the core of the anticyclonic eddy A1 (see Figure 4). Over a period of six consecutive days, from 13 to 19 February (Figure 2c), a diurnal mixed layer formed. A similar situation occurred between 24 and 27 February. The amplitude of variation of MLD between day and night can be as

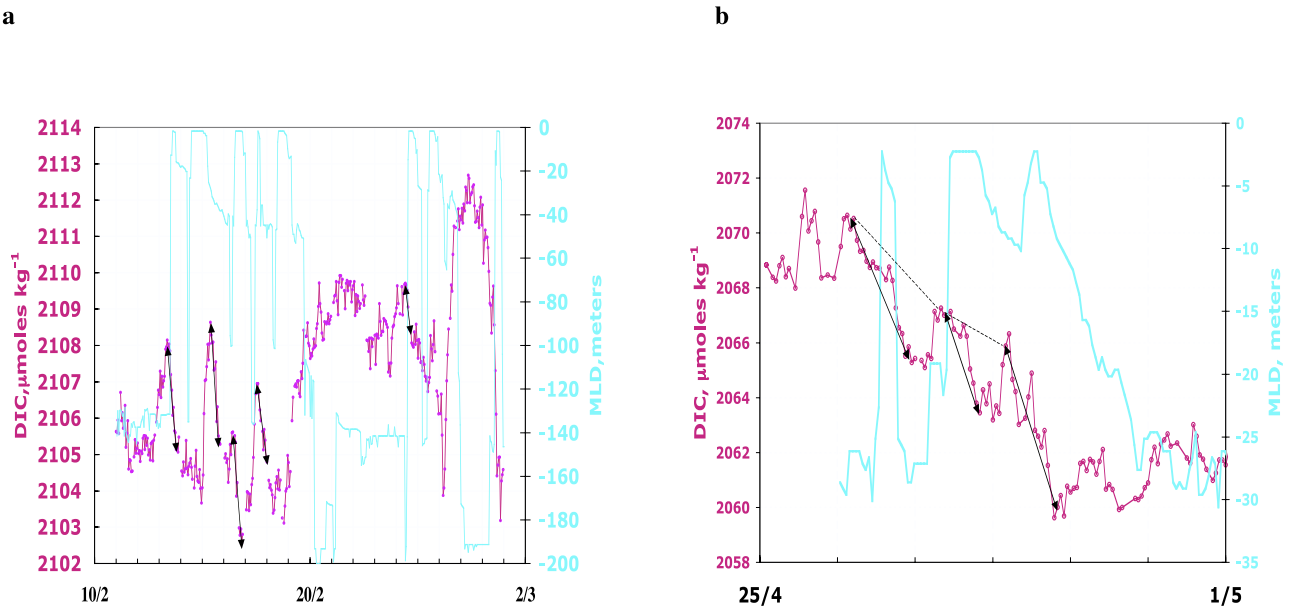

Figure 8. (a) Model MLD (cyan) in m and DIC (pink) in μmol kg^{-1} along the trajectory of the P4 buoy from 10 February to 1 March. (b) Same as Figure 8a for the P2b buoy between 25 April and 1 May.

large as 200 m (Figure 2a). The comparison between the model SST and the buoy data (Figure 2b) shows an associated diurnal temperature signal. On average, the maximum of the MLD and the minimum of SST take place one hour after sunrise, marking the end of maximum nighttime convection. The diurnal mixed layer is the shallowest and the SST maximum nine hours after sunrise. The observed maximum amplitude of the daily temperature variations is 0.3°C with a mean temperature of 13°C, which is reasonable for winter conditions in this region.

[32] During the POMME experiment, temperature profiles were made from drifting "Marisonde" surface buoys equipped with 100- to 200-m-long thermistor chains. The first temperature sensor was located at 2 m below the surface, and another ten sensors were evenly distributed along the length of the chain. MLD was estimated from hourly measurements of vertical profiles of temperature. Over the six successive days from 13 to 19 February, temperature measurements made by a Marisonde buoy less than 30 km from the P4 buoy show evidence of a diurnal mixed layer (data not shown). These observations are in very close agreement with the model results shown on Figures 2a and 2c. Observations along the trajectory of P2b buoy (Figure 2, right) are similar to those just discussed for the trajectory of P4 buoy, except that they describe the situation in the spring period. The general decrease of the mean MLD from 30 to 10 m between 26 April and 19 June is not smooth (Figure 2f). Periods of a few successive days with shallow diurnal mixed layers alternate with periods having a deeper MLD. One important conclusion based on the two situations analyzed above is that under certain conditions determined by the variability of the forcing atmospheric fluxes a stratification of the upper layers can be created even in winter.

[33] When a shallow diurnal mixed layer is formed (Figures 2 and 8), the predicted maximum value of SST in the afternoon is associated with a minimum of DIC. The opposite is true for the morning, on average one hour after sunrise. The simultaneous changes of SST and DIC measured by the P3 buoy are shown on Figure 9 at the end of March, over a three day period, to characterize the processes which drive the variability of DIC. C_M and C_m are the maximum and minimum values of DIC during one day. $\frac{\Delta C}{\Delta t}$ is the difference of two consecutive daily maxima of DIC.

[34] Biological processes, i.e., photosynthesis and respiration, and air-sea exchange are the mechanisms responsible for the change of DIC during one day, $(C_M - C_m)_{day-1}$, for two reasons: there is no mixing due to lateral advection as the buoy drifts in the same water mass, and a vertical contribution is excluded during the daylight part of the day whilst the mixed layer is shoaling. Primary production, PP, in μmol kg^{-1} day^{-1} and the air-sea flux F, in mmol m^{-2} day^{-1}. within the diurnal mixed layer (thickness h*) are the processes responsible for the drawdown and the uptake of DIC during the daylight period.

$$PP = (C_M - C_m)_{d^{-1}} + \frac{1}{\rho}\frac{F}{2h^*} \quad (3)$$

where h* is the thickness of the shallow diurnal mixed layer in m. ρ is the density of sea water. During the second part of the day, nocturnal convection mixes down the shallow mixed layer established during daylight, bringing cold and DIC rich deeper waters to the surface.

[35] $\frac{\Delta C}{\Delta t}$ is the change of DIC computed between 2 consecutive morning at the end of the nocturnal convection within the mixed layer (thickness h). $\frac{\Delta C}{\Delta t}$ represents the change of DIC within the mixed layer or Net Community

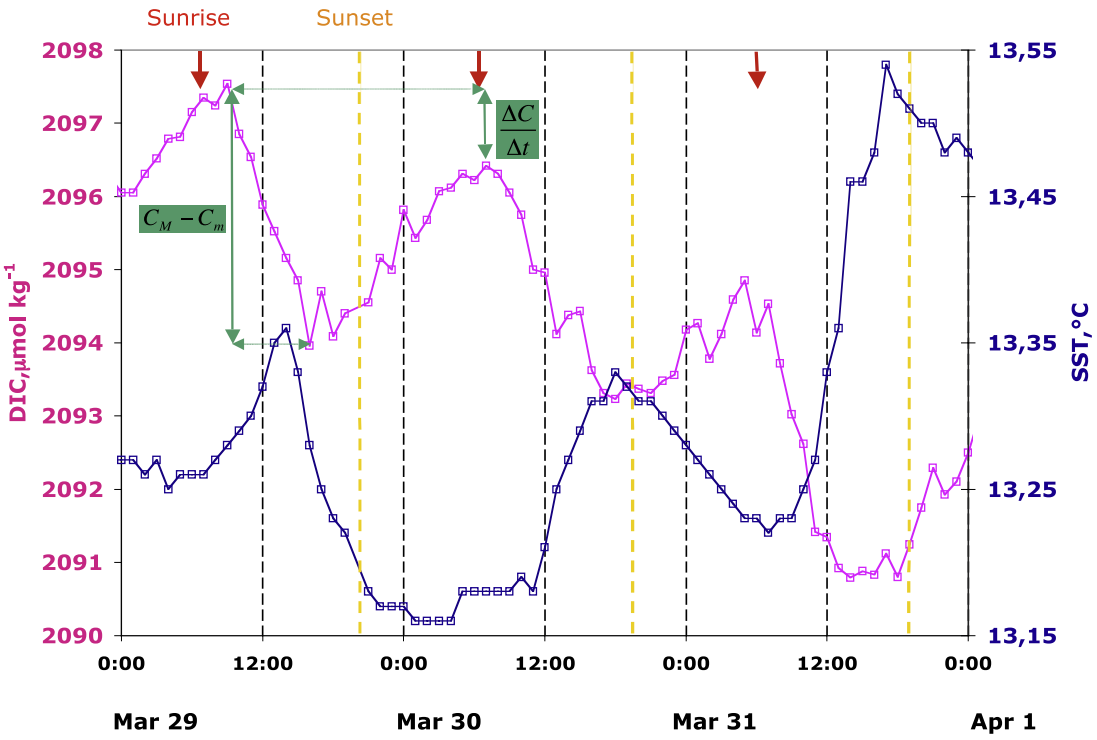

Figure 9. DIC (μmol kg^{-1}) and SST (°C) measured by the P3 buoy from 29 March to 1 April. The solid green arrows indicate the daily change of DIC from early morning to late afternoon ($C_M - C_m$) and the difference between two consecutive mornings ($\Delta C/\Delta t$). The hours of sunrise and sunset are indicated by the red and yellow arrows, respectively.

production, NCP in μmol kg^{-1} day^{-1} (the difference between the rate of gross C production, GCP, and metabolic CO_2, R, release over one day). We have

$$NCP = \frac{\Delta C}{\Delta t} + \frac{1}{\rho}\frac{F}{h} \quad (4)$$

where, h is the thickness of the diurnal mixed layer in m. Its maximum depth is assumed to be the same on the two consecutive days. This is shown for instance on Figure 2c between 13 and 16 February. No contribution of vertical advection at the base of the mixed layer has to be taken account. With equations (3) and (4), we compute PP at −2 m and NCP integrated on the MLD from the hourly measurements made along the trajectories of the CARIOCA buoys.

[36] In order to further compare the in-situ biological production rates deduced from the buoy data with the measurements made in the field by classical in vitro techniques, like ^{14}C or ^{13}C or O^{17}, O^{18} incubations, which are not only performed from dawn to dusk, (Primary Production, PP), but also from dawn to dawn, we compute the gross community production (GCP). We have

$$GCP = PP + \frac{R}{2} \quad (5)$$

The respiration rate is assumed to be constant during a 24-hour day [*Robinson et al.*, 2002]. To estimate GCP, at −2 m, we assume that NCP at −2 m is identical to the value integrated on the MLD. We have

$$GCP = NCP + R \quad (6)$$

or

$$GCP = 2(C_M - C_m)_{d^{-1}} - \frac{\Delta C}{\Delta t} + \frac{1}{\rho}\frac{F}{h^*}\left(1 - \frac{1}{a}\right) \quad (7)$$

with

$$h = ah^* \quad (8)$$

In equations (3) to (8), $(C_M - C_m)_{day-1}$, $\frac{\Delta C}{\Delta t}$, F are three quantities experimentally determined with the buoy data. The diurnal signals $(C_M - C_m)_{day-1}$ and $\frac{\Delta C}{\Delta t}$ are computed from hourly measurements of fCO_2 and salinity. The terms h^* and a are estimated from the mixed layer model.

[37] It is important to recognize that these estimates of the biological rates calculated from the observed high-frequency buoy measurements at a depth of 2 m are only valid when there is evidence of the establishment of a diurnal mixed layer as shown by the signature of a diurnal SST and DIC signal. In addition, these estimates also assume no horizontal advection between two consecutive days or vertical mixing during the shoaling of the mixed layer. From the temporal variation of the diurnal mixed layer estimated by

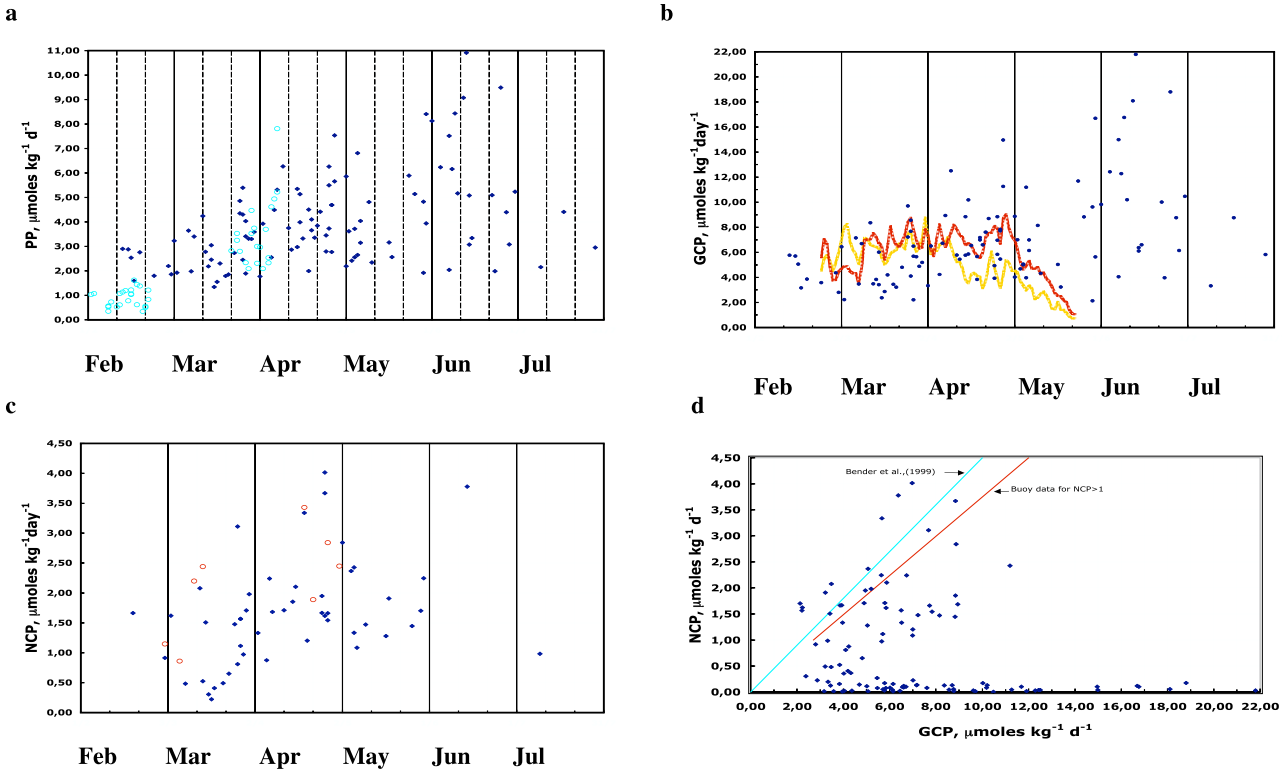

Figure 10. Time variation of (a) PP in μmol kg^{-1} day^{-1}. Buoy data in blue; isotopic 12-hour incubations, ^{13}C in cyan. (b) GCP in μmol kg^{-1} day^{-1}. Buoy data in blue; 4-D model, north of 40.5°N (red); south of 40.5°N (yellow). (c) NCP in μmol kg^{-1} day^{-1}. Buoy data in blue; isotopic 24-hour incubations, ^{14}C, in red. (d) NCP versus GCP. The slope of the red line is 0.37 (see text).

the model as shown in Figures 2 and 8, it is clear that no simple statistical treatment can be used to select the days of interest. This lack of predictability results from the high-frequency variability of atmospheric forcing in this area over the timescale of our study.

[38] We have identified a set of 107 days for which a maximum of DIC, C_M at the hour of sunrise ±1 hour and a minimum, C_m, 12 ± 1 hours later have been observed. A day-to-day change $\frac{\Delta C}{\Delta t}$ could be simultaneously observed in 51 cases. The maximum values of $(C_M - C_m)_{day-1}$ and $\frac{\Delta C}{\Delta t}$ are, respectively, 11 and 4 μmol kg^{-1} $_{day-1}$. The values of the minimum and maximum depth of the diurnal mixed layer to be used in equations (3) to (8) are estimated from the results of the 1-D model as seen on Figures 2a and 2d. h* and h, are, respectively, equal to 10 and 75 m for a winter situation or 5 and 15 m for a late spring season. The maximum input of DIC due to air-sea exchange in the surface layer is equal to 0.35 μmol kg^{-1} day^{-1}, 1.1 μmol kg^{-1} day^{-1} and 1.8 μmol kg^{-1} day^{-1}, respectively, for NCP, PP and GCP. On average, the relative contribution of the air-sea flux to PP, GCP and NCP is, respectively, 8%, 13% and 20%.

[39] PP, NCP and GCP display a large variability superimposed upon a general increasing trend from February to mid/late June (Figures 10a–10c). Figure 10d shows the distribution of all the values of NCP and GCP. For about half of the estimates (56 days out of 107), no day-to-day change of DIC has been detected, and consequently NCP is close to zero, even though GCP can be large. This can be the case in an oceanic ecosystem in which photosynthesis and respiration are in balance. The slope of the dotted line, equal to 0.37 ± 0.17, represents the ratio NCP/GCP for the 38 days when NCP is larger than 1 μmol kg^{-1} day^{-1}.

3.3.2. Comparison With Results of In Vitro Isotopic Methods and Model

[40] During the POMME surveys at sea, measurements of in vitro biological production have been made either using the isotopic ^{13}C technique on the first cruise legs [*Fernández et al.*, 2005a], or the ^{14}C technique during the second cruise legs [*Claustre et al.*, 2005]. These isotopic measurements were performed over four successive time intervals of ~twenty days from the beginning of February to the beginning of May within the POMME domain.

[41] In the first case, samples were collected during the hydrographic stations before sunrise at six standard depths between 5 m and 80 m and then labeled with ^{13}C. Incubations using appropriate light screens were done on deck over a period of twelve hours from dawn to dusk. The results of the measurements at 5 m are compared to the distribution of PP deduced from the buoy data in Figure 10a. It should be kept in mind that the results from these twelve hour long incubations do not account for the respiration of heterotrophs, and only partially for that of autotrophs, and thus could be larger than the PP estimates given by equation (3). During the second leg of the POMME cruises, which focused on process studies at four stations, in-situ primary production measurements were performed using the ^{14}C method. Samples were collected before sunrise between

5 and 80 m, inoculated with ^{14}C and then incubated in situ for 24 hours. In such conditions, ^{14}C fixed into organic particles is considered to estimate net community production [*Marra*, 2002]. The distribution of GCP calculated along the trajectories of the drifters using equation (6) are compared in Figure 10b with the results of a 3-D high-resolution biophysical coupled model of the POMME region dedicated to the study of the submesoscale variability of primary production during late winter and spring [*Lévy et al.*, 2005]. The initially nitrogen-based model has been enhanced with a carbon chemistry module, and a constant C:N ratio equal to 10 has been taken into account [*Resplandy et al.*, 2009; *Kortzinger et al.*, 2001]. The two curves on Figure 10b show the time evolution of the model average GCP north and south of 40.5°N. After mid April, we notice that mean production rates are far larger, up to a factor three, north of the front at 40.5°N. The smaller range of variability of the model results compared to the buoy data is expected since the model represents an area average. The magnitude and the mean trend of the GCP from model calculations and buoy GCP data are in quite good agreement until the beginning of May. After this point, the decreasing trend of GCP predicted by the model is not supported by the individual daily buoy data, which increase until mid June.

3.3.3. Discussion

[42] The biological production rates, PP, estimated with the buoy data show an increasing trend from February to June (Figure 10a). The results of the ^{13}C assimilation technique show the same trend between February and April. The values of PP computed in February are small, lower or equal to 1 μmol kg^{-1} day^{-1} for the ship data or 3 μmol kg^{-1} day^{-1} for the buoy data. At this period of the year, a bias toward higher values of the estimation of PP with the buoy measurements can be expected as a surface DIC change, $(C_M - C_m)_{day-1}$, must preferentially be observed on clear and sunny days when a warm diurnal layer forms. At the time of the spring cruise (26 March–13 April), the range of variability of PP measured by the two techniques is very similar showing a change of a factor up to three within two consecutive days, demonstrating how biological production is highly modulated by temporal variability during the spring bloom period. Figure 10c shows the NCP rates deduced from eight ^{14}C assimilation experiments made at four stations during each second leg of the winter and spring cruises and from the measurements of the buoys. Values of NCP <1 μmol kg^{-1} day^{-1} indicate that metabolic and air-sea exchange processes are close to being in balance over a day. A clear increase in NCP rates is observed for the whole set of data starting in early March, which seems to be a period of significant production prior to the expected start of the spring bloom. The maximum values of NCP observed between 21 and 26 April are associated with the development of a secondary bloom just after an atmospheric depression passes over the north of the POMME area. It was responsible for the partial destratification of the water column, the deepening of the MLD and a subsequent reinjection of nutrients into the mixed layer, which was depleted previous to the storm [*Lévy et al.*, 2005]. This again emphasizes the role of short-term phenomena in the control of biological drawdown of carbon in the upper layers of the ocean, mainly driven by variability in solar radiation, small scale temporal variability of atmospheric forcing and ocean mesoscale dynamics.

[43] Determined both by in vitro isotopic incubation, the values of PP are larger than NCP (Figures 10a and 10c) as expected since the overnight loss of organic carbon due to ecosystem respiration is not measured in dawn to dusk incubation experiments. This difference can be estimated by the buoy data using equations (3) and (4). The relative distribution of the two production rates, NCP and GCP, depends of the net autotrophic metabolism of the oceanic ecosystem. The estimation of the NCP/GCP ratio is the subject of debate in the literature. It is acknowledged that ^{14}C assimilation (twenty four hours) estimates net production while $^{18}O_2$ method gives a good estimate of gross photosynthesis [*Marra*, 2002; *Bender et al.*, 1999; *Hendricks et al.*, 2004]. With the buoy data, we have direct access to these production rates measured in situ. Figure 10d shows all the values of NCP as a function of GCP. The mean value of the ratio NCP/GCP is equal to 0.37 when NCP is $\geq$1. A value of "about 0.45" has been calculated on the basis of the experiments made during the JGOFS equatorial Pacific experiment [*Bender et al.*, 1999]. The overall variability of the NCP/GCP ratio is an indication of the difference between the rates of photosynthesis and respiration of the oceanic ecosystem. Direct and autonomous measurement of new production based on time series observations with autonomous nitrate sensors deployed on oceanographic moorings offshore of Monterey Bay, California also illustrate the high-frequency intermittency in biological production events [*Johnson et al.*, 2006]. Variable diurnal cycles of surface fCO_2 measured in the equatorial Atlantic and Pacific Ocean have also previously been attributed to the combined effects of diel changes in temperature, stratification, biological activity, and oceanic CO_2 release from a shallow daytime mixing layer [*Bakker et al.*, 2001; *DeGrandpre et al.*, 2004].

3.4. Averaged NCP over the March, April, and May Period

3.4.1. Buoy Data

[44] We here attempt to derive an integrated mean value of NCP over the three month period from March to May, taking advantage of the continuous DIC concentrations derived from the buoy data (Figure 11). Over this period, the two P1 and P4 buoys drifted successively eastward then westward at the mean latitude of 42 ± 1.5°N (Figure 1b). The mean slope $\frac{\Delta C}{\Delta t}$ of the linear regression computed for the DIC concentrations calculated from the P1 and P4 buoys are 0.38 and 0.34 μmol kg^{-1} day^{-1}, respectively, for the same 3-month interval.

[45] If $\overline{F_{bio}}$ and $\overline{F_c}$ in mmol m^{-2} day^{-1} represent the mean biological drawdown rate and air-sea flux in the mixed layer over this period, we have

$$\overline{F_{bio}} = \overline{H}.\frac{\overline{\Delta C}}{\Delta t} - \overline{F_C} \tag{9}$$

[46] In the equation (9), H, in m, represents the mean value of the MLD. A Revelle factor equal to 10.7 is used [*González Dávila et al.*, 2005, Table 2] to derive the value

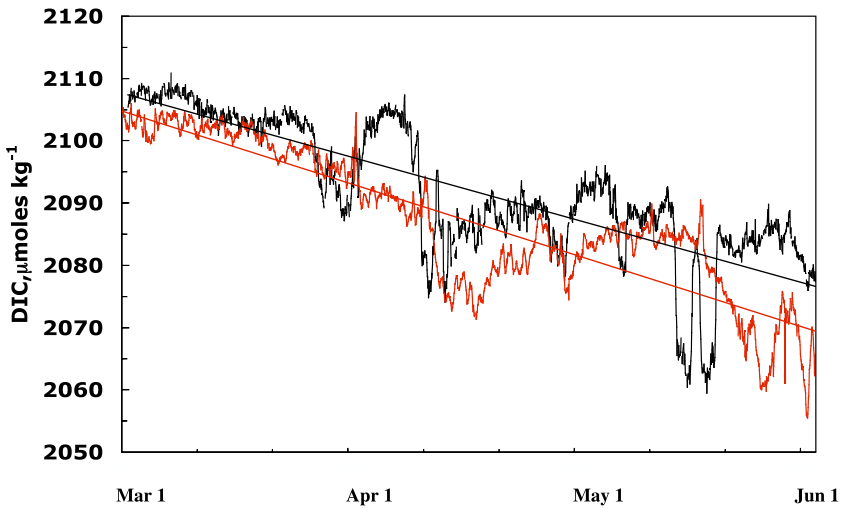

Figure 11. Change of DIC in μmol kg^{-1} from 1 March to 1 June for the P1 buoy (red) and the P4 buoy (black). The slopes of the regression lines are, respectively, 0.38 and 0.34. μmol kg^{-1} day^{-1}.

of the influx of DIC in the mixed layer due to air-sea exchange, F_C, from the CO_2 gas flux, F_G, measured by the buoys. On average, for the range of values of fCO_2 and DIC measured by the buoys, we have $F_C/F_G = 1/1.8$.

[47] For the March–May period, the values of F_C are 3.14 and 2.27 mmol m^{-2} day^{-1}, respectively, for the P1 and P4 buoys. The signs of F_{bio} (a drawdown), and F_c (an intake) are opposite. The numerical form of the equation (9) becomes

$$\text{for P1}, \overline{F_{bio}} = 0.38\overline{H} + 3.14 \quad (10)$$

$$\text{and for P4}, \overline{F_{bio}} = 0.34\overline{H} + 2.27 \quad (11)$$

The annual cycle of the mixed layer depth has been estimated during the POMME experiment from a study of the annual sea surface heat budget [*Caniaux et al.*, 2005b]. Stratification begins around 20 March; the mean value of H between 1 March and 1 June is equal to 75 m. From equations (10) and (11), we compute for the P1 buoy, F_{bio} = 31.6 mmol m^{-2} day^{-1} and for the P4 buoy, F_{bio} = 27.8 mmol m^{-2} day^{-1}. The relative importance of the gas flux compared to the biological fluxes is equal to 10% and 8%, respectively, for the two buoys.

[48] The term $\frac{\overline{F_{bio}}}{\overline{H}}$ can be interpreted as a mean value of NCP over the March–May period in the mixed layer. From the P1 buoy we calculate 0.42 μmol kg^{-1} day^{-1} and for the P4 buoy, 0.37 μmol kg^{-1} day^{-1}. These values are on the low side of the range of data based on the daily measurements made by the buoys, as shown on Figure 10c. Consequently, this again indicates that the time averaged mean productivity computed over a 3-month period is due to high temporal and spatial frequency production events instead of the result of a regular production regime.

3.4.2. Comparison With Results of Other Methods

[49] An average model estimation of new production inside the POMME study area between 22 February and 31 May 2001 is provided in Table 2 of *Lévy et al.* [2005], using a standard Redfield ratio. *Resplandy et al.* [2009] have shown that the appropriate value of the ratio C/N is 10 in the POMME area in February–May, similar to the value previously proposed by *Kortzinger et al.* [2001] in the north Atlantic. The model estimation of new production is then equal to 32.3 mmol C m^{-2} day^{-1}. The time period considered in the model run is similar to the 1 March–31 May time lapse used in the analysis of buoy data. The close agreement between the results of the model and the buoy data is surprising given the high variability of the spring bloom on short temporal and spatial scales. However, both approaches represent an integration over the three months period, and thus the temporal variability is smoothed.

[50] On the basis of the results of a dual $^{13}C/^{15}N$ isotopic technique used to estimate carbon and nitrogen uptake rates, an annual carbon new production for the entire POMME region has been estimated to be 15.6 mmol m^{-2} day^{-1}, with a value for winter (49 days) equal to 16 mmol m^{-2} day^{-1} and for spring (59 days) equal to 48 mmol m^{-2} day^{-1} [*Fernández et al.*, 2005b, Table 3]. After weighing by the number of days of each season, we compute a mean value of NCP corresponding to the winter and spring POMME cruises period equal to 33.5 mmol m^{-2} day^{-1}. This estimation is again in close agreement with both the model and the buoy data.

[51] Biological drawdown is principally responsible for the decreasing trend of DIC shown on Figure 3; the vertical excursions of the values around this trend are caused by the dynamic mixing processes of mesoscale eddies and temporal variability along the routes of the drifters.

3.4.3. Control of Surface fCO_2 by Biology, Thermal Heating, and Gas Exchange

[52] Along the trajectory of P1 and P4 buoys, respectively, we have calculated a mean biological drawdown of DIC over the 3 months period, March–May, equal to 0.42 μmol kg^{-1} day^{-1} and 0.37 μmol kg^{-1} day^{-1}. The incoming gas flux has been estimated to 0.04 μmol kg^{-1} day^{-1} and 0.03 μmol kg^{-1} day^{-1}, respectively, for the two buoys. A mean value of the ratio of the associated changes of fCO_2 and DIC equal to 1.8 μatm/μmol kg^{-1} has been calculated. Then, if we consider mean numbers on the basis of the 2 buoys data, the change of fCO_2 due to biology is -0.71 μatm day^{-1}, and the contribution of the air sea flux is +0.06 μatm day^{-1}.

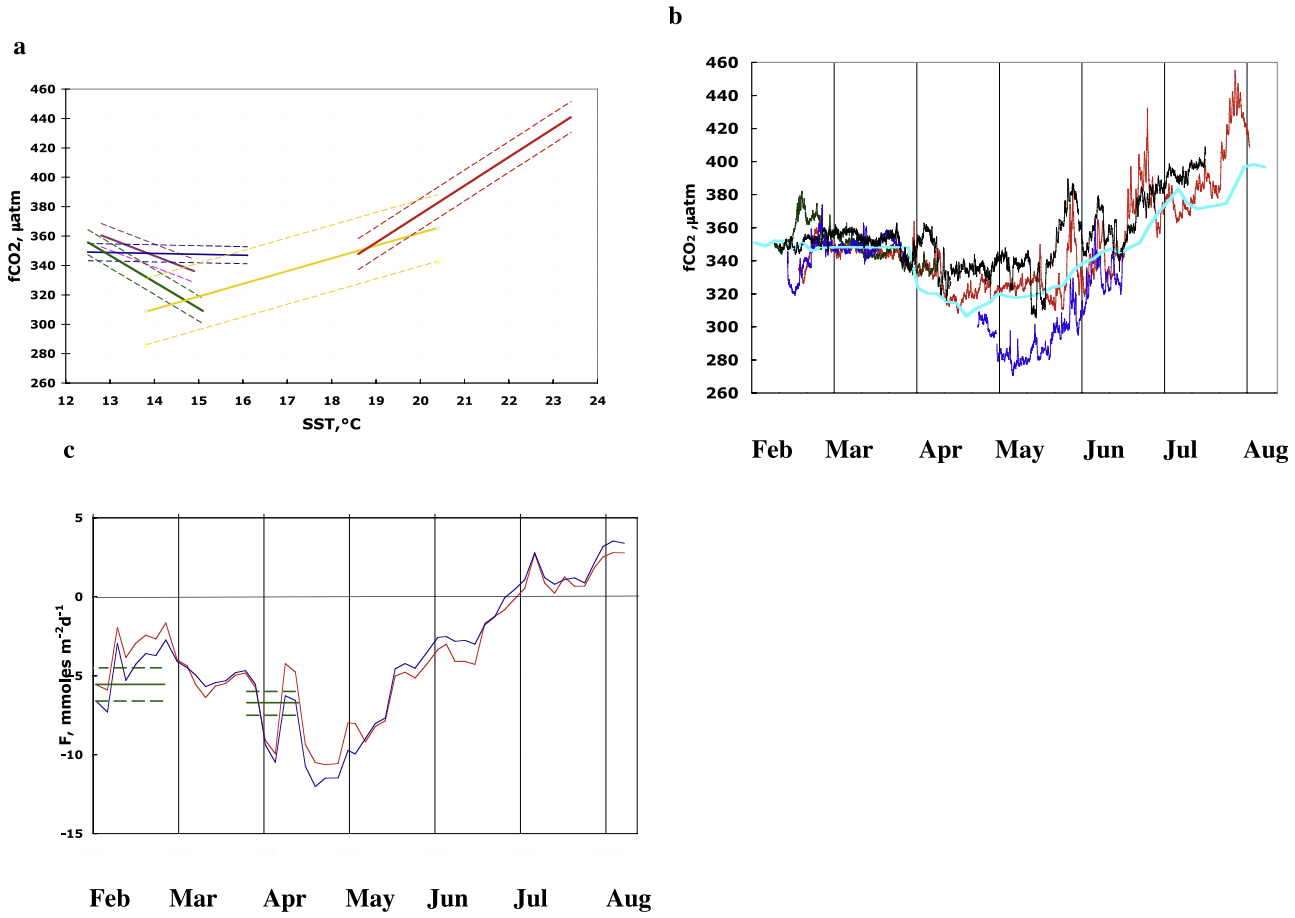

Figure 12. (a) fCO_2/SST relationships for five periods: February (purple), March (blue), April (green), May–19 June (yellow), 20 June–1 August (red). The dotted lines indicate ±1 σ. (b) fCO_2 in μatm measured by the four buoys (same color code as in Figure 1b). The cyan line shows the interpolated values using satellite SST. (c) Air-sea CO_2 flux in mmol m^{-2} day^{-1} calculated over the POMME zone, 39°N/45°N–16°W/21°W (red), and on the enlarged zone, 36°N/46°N–12°W/22°W (blue). Each data point represents a 3–4 daytime interval. The green lines have been calculated by González-Dávila et al. using ship data. The full green line shows the mean value over the POMME zone. The dotted ones refer to the northern part, north of 42°N, and the southern one, south of 42°N. Negative values indicate that the ocean is a sink for atmospheric CO_2.

[53] A regular increase of SST is measured by the 2 buoys between 1 March and 20 May. Its mean value is equal to 0.019° day^{-1}, corresponding to a fCO_2 change of +0.27 μatm day^{-1} (thermal heating factor, 4.23%/°C). Over the same 80 days period, a mean decrease of fCO_2 equal to 32 μatm., i.e., a gradient equal to −0.40 μatm day^{-1}, is measured. This number agrees with the sum of the individual contributions of biology, gas exchange and thermal heating equal to −0.38 μatm day^{-1}. Thus the overall balance of the factors which control the variability of surface fCO_2 shows that the air-sea flux contribution is small, while the thermal heating effect is dominated by biology at this period of the year.

4. Carbon Budget of the POMME Area

4.1. CO_2 Air-Sea Flux

4.1.1. Integration Over the POMME Region

[54] One of our objectives is to estimate the CO_2 gas flux, F_{CO2}, exchanged at the air-sea interface from February to August over the POMME area. In order to spatially extrapolate over the POMME area the measurements of fCO_2 made at the sea surface along the trajectories of the buoys (Figure 3a), we derive quasi-monthly (1 to 1.5 month interval) linear least squared regressions between fCO_2 and SST on the basis of the hourly measurements of the four buoys. Then we use satellite-derived temperature data and these linear SST-fCO_2 regressions to produce fCO_2 maps over the POMME region. These are then combined with maps of the gas exchange coefficient computed using QSCAT wind speeds to estimate F_{CO2} (equation (1)).

[55] Figure 12a represents the fCO_2/SST relationships corresponding to five time intervals: February, March, April, May–19 June, and 20 June–31 July. The values of the standard deviation of fCO_2 with respect to each fit vary between 7 and 9 μatm, except for the May–19 June period when it is equal to 20 μatm. It is worthwhile to point out that, whereas the range of variability of SST is about the same for the February, March and April period, the fCO_2/SST relationships are different. This results from the bio-

logical uptake of CO_2, which becomes important in April (Figure 3), and so it is not appropriate to compute a unique relationship for these two periods. The slope of the June–July relationship, equal to 18.3 μatm/°C, is very close to the relationship expected from thermal heating on the value of fCO_2 equal to 4.23%/°C or 17 μatm, which is expected to be the dominant factor controlling the variability of fCO_2 during this oligotrophic period. There are several reasons for the poor quality of the fit for the May–mid June period. Four factors control the distribution of fCO_2: thermal heating, biological consumption, air-sea exchange and mixing events. While the positive slope of the regression line indicates that the thermal factor might dominate, the large variation of the data points is most likely the result of the large spatial and temporal inhomogeneity of biological processes as already observed in the distribution of DIC.

[56] SST fields derived at NOAA/NESDIS from AVHRR data interpolated twice a week at 0.5° resolution (http://www.osdpd.noaa.gov/PSB/EPS/SST/sst_anal_fields.html) were used to compute the temporal distribution of fCO_2 averaged over the POMME domain (Figure 12b). A difference between the calculated and observed values in the June–July period is expected since the buoys only sampled the southern part of the domain from 40°N to 37°N during this period. The relatively abrupt change for the calculated values around 1 April results from the change of the fCO_2/SST relationship used after the end of March. To compute the gradient $(\Delta fCO_2)_{sea\text{-}air}$ in equation (1), the values of fCO_{2air} have been averaged over the same time interval as the NOAA SST used to compute fCO_2 at the sea surface.

[57] Maps of the gas exchange coefficient, K, at weekly and 1° × 1° resolution have been derived from level 2 QSCAT wind speeds at 25km resolution (NASA/JPL nudged product; rain flagged wind speeds discarded) using the extrapolation method described in [*Boutin and Etcheto*, 1997]. K is significantly smaller during the summer months compared to the winter months, and there is a factor of ~3 between the values calculated in March and July.

[58] Interpolated values of the flux, F, averaged over three or four days are reported in Figure 12c. Two geographical regions have been considered, the original POMME zone (39°N–45°N/16°W–21°W) and the larger area explored by the buoys (36°N–46°N/12°W–22°W). The fluxes are not very different (the mean difference is 2.5%) notwithstanding a factor 3.4 in area between the two domains.

4.1.2. Comparison With Other Results

[59] Over the POMME area, the mean air-sea flux over the February to August 6-month period is equal to 4 mmol m^{-2} day^{-1}. The uptake is maximum, close to 10 mmol m^{-2} day^{-1}, in April–May mainly driven by the large biological drawdown of carbon. After the beginning of July, the ocean becomes a source of CO_2 to the atmosphere. However, the CO_2 outflux is not large because of the low wind regime prevailing at this period of the year.

[60] The net sea-air CO_2 flux has been estimated by *González Dávila et al.* [2005] using the measurements of $(\Delta fCO_2)_{sea\text{-}air}$ made along the ship track during the first legs of the winter and spring POMME cruises and using the ECMWF wind data to compute the exchange coefficient. The agreement with the interpolated buoy data is satisfactory (Figure 12c), particularly for the spring cruise during which the development of the bloom created a large spatial and temporal heterogeneity of the distribution of fCO_2 at the ocean surface.

[61] We have compared our data to the values of the sea-air fCO_2 difference, $(\Delta fCO_2)_{sea\text{-}air}$ given in the recent climatology of *Takahashi et al.* [2007] assumed to represent conditions for the year 2000 centered on the area bounded by the latitudes 38°N and 46°N, and the longitudes 15°W and 20°W, which is quite close to the POMME study area. The mean of the six monthly values of $(\Delta fCO_2)_{sea\text{-}air}$ from February to August is equal to −28.6 μatm. The equivalent quantity based on the interpolation of the buoy data from February to August 2001 is −22.9 μatm. If the difference between the mean values is only 20%, it hides temporal discrepancies as the monthly distribution of the 2 sets of $(\Delta fCO_2)_{sea\text{-}air}$ values is different. In April–May, the maximum amplitude of $(\Delta fCO_2)_{sea\text{-}air}$ due to the biological drawdown of fCO_2 is equal to −40 μatm for the climatology while it is equal to −60 μatm with the buoy measurements. The outgassing shown by the buoy data starting at the end of June is not observed in the climatology. A similar discrepancy is also found for the September 2001 data [*González Dávila et al.*, 2005]. The mean value of $(\Delta fCO_2)_{sea\text{-}air}$ measured during the fall cruise of the ship is equal to +15 μatm, while in the *Takahashi* climatology it is equal to −11 μatm. The absence of summer CO_2 outgassing in the climatology is somewhat surprising but it may be attributed to different heat storage in the upper ocean surface layer between the climatology and the year 2001. *Caniaux et al.* [2005b] showed (Figure 5a) that the mean SST over the POMME region is higher than the climatology during the summer months.

4.2. Subduction of Atmospheric Anthropogenic Carbon During Winter

[62] On the basis of the synthesis of the physical data collected during the POMME experiment, *Gaillard et al.* [2005] investigated the subduction mechanisms of the subpolar mode water formed in winter in this area of the northeast Atlantic. From the analysis of the averaged depth and density of the mixed layer over the period of maximum depth (6–20 March), they show that a large volume of subducted water with density slightly above 26.9 kg m^{-3} was formed north of 42.5°N. The subpolar mode water is continuously advected southward across the 42°N latitude. The resulting annual mean transport reaches 1.4 10^6 m^3 s^{-1} (1.4 Sverdrup), which corresponds to an approximate subduction rate of 120 m yr^{-1}.

[63] Density time series are calculated from the temperature and salinity measurements made hourly by the CARIOCA buoys. In Table 2, we summarize the density and DIC content over the winter period in the latitude range of the buoys, from the time of the deployment of the drifters in February until the end of March. The density is smaller in the southern than in the northern part of the zone and the onset of stratification is observed earlier, around 8 March.

[64] In the northern part of the zone, in the latitude range 43°N–44°N, the mean density measured by P3 and P4 buoys is equal to 26.96 kg m^{-3} while the individual values are all above 26.9 kg m^{-3}. Stratification begins around 20 March, in agreement with the time change of the MLD proposed by *Caniaux et al.* [2005b]. We see that, over the same time period and in the same latitude band, the

Table 2. February–March Average Potential Density and DIC Observed for the Four Buoys

Buoy	Latitude °N Range	Onset of Stratification	Mean Density (kg m^{-3}) Before Stratification	Mean DIC (μmol kg^{-1}) Before Stratification
P1	41	21 Mar.	26.84	2102
P2	40.5 → 38.8	8 Mar.	26.77	2097
P3	44	20 Mar.	26.96	2108
P4	43	20 Mar.	26.96	2103

density measured by the buoys corresponds well with the properties of the shallow mode water that is subducted following the mechanism proposed by *Gaillard et al.* [2005]. The annual amount of carbon which will be transported below the seasonal mixed layer is estimated to be equal to 1.1×10^{15} g yr^{-1} of carbon (or 1.1 PgC yr^{-1}) as the mean subduction rate is equal to 1.4 Sverdrup and the average DIC content of the subducted water equal 2105 μmol kg^{-1}.

[65] The formation and transport of mode water and intermediate waters is the primary mechanism for moving atmospheric anthropogenic CO_2 to intermediate depths. The North Atlantic basin is a major player as it stores 23% of the global oceanic anthropogenic CO_2 calculated over the period 1800 to 1994 [*Sabine et al.*, 2004]. *Pérez et al.* [2002] calculated the contribution of anthropogenic carbon, C_{ANT}, in a section across the Eastern North Atlantic from 35°N to 63°N along 20°W (Oaces NAtlIIB-93, July/August 1993). For the potential density surface interval between 26.9 and 27 kg m^{-3}, they indicate a value of C_{ANT} equal to 45 ± 4 μmol kg^{-1}. This would be equal to 53 μmol kg^{-1} in the year 2001 if we assume a mean annual increase of C_{ANT} equal to 1 μmol kg^{-1} as determined at the ESTOC time series station [*González–Dávila et al.*, 2007]. Thus 2.8×10^{13} gC yr^{-1} of anthropogenic carbon would be subducted in the POMME region in the upper 300 to 500 m of the water column. In a recent paper, *Paci et al.* [2007] proposed a value of 0.8 Sv for the mean subduction rate of water instead of 1.4Sv as estimated by *Gaillard et al.* [2005]. The amount of carbon, natural and anthropogenic, would be 57% of the numbers indicated above. In either case, it appears that the formation of mode water in the POMME area in the northeast Atlantic is an efficient mechanism for removing anthropogenic CO_2 from the ocean surface to intermediate waters, which subsequently become isolated from the influence of the atmosphere on decadal timescales.

5. Summary and Conclusions

[66] High-frequency (hourly) measurements of surface fCO_2 and estimated DIC have been provided by four Lagrangian CARIOCA buoys deployed in the POMME area between February and August 2001. The main findings inferred from the analysis of the data are as follows.

[67] 1. In winter, sharp gradients of surface fCO_2, up to 25 μatm over 40 km, are present owing to an intense submesoscale variability dominated by advection and stirring induced by the presence of eddies and filaments along the routes of the drifters. This is consistent with results of a submesoscale model presented by *Resplandy et al.* [2009].

[68] 2. Diel measurements of DIC provide direct in-situ measurements of NCP, PP and GCP starting in February. A comparison with in vitro data indicates that episodic biological production processes are triggered by the mesoscale activity of surface eddies which is not always captured by traditional sampling strategy.

[69] 3. The POMME area is on average a sink for atmospheric CO_2 equal to 4 mmol m^{-2} day^{-1} between February and August 2001. The uptake of atmospheric CO_2 is maximum in April driven by the biological drawdown of carbon; outgassing is observed after the end of June.

[70] 4. Anthropogenic carbon is subducted in the subpolar mode water around 20 March in the north of the area. It amounts to 2.8×10^{13} gC yr^{-1} or 1.6×10^{13} gC yr^{-1}depending on the value of subduction rate; namely, 1.4 Sv or 0.8 Sv. These results highlight the specific role of the POMME area within the North Atlantic basin since it is both a sink for atmospheric CO_2 as well as an area of mode water formation, which carries anthropogenic carbon from the ocean surface to intermediate waters.

[71] **Acknowledgments.** This work was supported by the French programs PROOF and PATOM (CNRS/INSU). The PIs of the POMME program, Laurent Mémery and Gilles Reverdin, are warmly acknowledged for their deep investment in all phases of the project and especially for providing us access to a unique set of data and results. Special thanks to Yves Dandonneau who has put forward his expertise in marine biology in every constructive discussions. We are grateful to the technical division of INSU, in particular L. Beaumont and T. Danguy, for the preparation of the CARIOCA buoys. The critics and comments of three reviewers have been very helpful in improving the manuscript.

References

Bakker, D. C. E., J. Etcheto, J. Boutin, and L. Merlivat (2001), Variability of surface-water fCO_2 during seasonal upwelling in the equatorial Atlantic Ocean as observed by a drifting buoy, *J. Geophys. Res.*, *106*, 9241–9254.

Bender, M. J., Orchardo, M.-L. Dickson, R. Barber, and S. Lindley (1999), In vitro O_2 fluxes compared with ^{14}C production and other rate terms during the JGOFS Equatorial Pacific experiment, *Deep Sea Res. Part I*, *46*, 637–654.

Bouruet-Aubertot, P., H. Mercier, F. Gaillard, and P. Lherminier (2005), Evidence of strong inertia-gravity wave activity during the POMME experiment, *J. Geophys. Res.*, *110*, C07S06, doi:10.1029/2004JC002747.

Boutin, J., and J. Etcheto (1997), Long term variability of the air-sea CO_2 exchange coefficient: Consequences for the CO_2 fluxes in the equatorial Pacific Ocean, *Global Biogeochem. Cycles*, *11*, 453–470.

Caniaux, G., A. Brut, D. Bourras, H. Giordani, A. Paci, L. Prieur, and G. Reverdin (2005a), A 1 year sea surface heat budget in the northeastern Atlantic basin during the POMME experiment: 1. Flux estimates, *J. Geophys. Res.*, *110*, C07S02, doi:10.1029/2004JC002596.

Caniaux, G., S. Belamari, H. Giordani, A. Paci, L. Prieur, and G. Reverdin (2005b), A 1 year sea surface heat budget in the northeastern Atlantic basin during the POMME experiment: 2. Flux optimization, *J. Geophys. Res.*, *110*, C07S03, doi:10.1029/2004JC002695.

Claustre, H., M. Babin, D. Merien, J. Ras, L. Prieur, S. Dallot, O. Prasil, H. Dousova, and T. Moutin (2005), Toward a taxon-specific parameterization of bio-optical models of primary production: A case study in the North Atlantic, *J. Geophys. Res.*, *110*, C07S12, doi:10.1029/2004JC002634.

Copin-Montegut, C., M. Begovic, and L. Merlivat (2004), Variability of the partial pressure of CO_2 on diel to annual time scales in the Northwestern Mediterranean Sea, *Mar. Chem.*, *85*, 169–189.

DeGrandpre, M. D., R. Wanninkhof, W. R. McGillis, and P. G. Strutton (2004), A Lagrangian study of surface p CO_2 dynamics in the eastern equatorial Pacific Ocean, *J. Geophys. Res.*, *109*, C08S07, doi:10.1029/2003JC002089.

Fernández, C. I., P. Raimbault, G. Caniaux, N. Garcia, and P. Rimmelin (2005a), Influence of mesoscale eddies on nitrate distribution during the POMME program in the northeast Atlantic Ocean, *J. Mar. Syst.*, *55*, 155–175.

Fernández, C. I., P. Raimbault, N. Garcia, P. Rimmelin, and G. Caniaux (2005b), An estimation of annual new production and carbon fluxes in the northeast Atlantic Ocean during 2001, *J. Geophys. Res.*, *110*, C07S13, doi:10.1029/2004JC002616.

Gaillard, F., H. Mercier, and C. Kermabon (2005), A synthesis of the POMME physical data set: One year monitoring of the upper layer, *J. Geophys. Res.*, *110*, C07S07, doi:10.1029/2004JC002764.

Gaspar, P., Y. Grégoris, and J. M. Lefèvre (1990), A simple eddy kinetic energy model for simulations of the oceanic vertical mixing: Tests at station Papa and long-term upper ocean study site, *J. Geophys. Res.*, *95*, 16,179–16,193.

Giordani, H., G. Caniaux, L. Prieur, A. Paci, and S. Giraud (2005), A 1 year mesoscale simulation of the northeast Atlantic: Mixed layer heat and mass budgets during the POMME experiment, *J. Geophys. Res.*, *110*, C07S08, doi:10.1029/2004JC002765.

González Dávila, M., J. M. Santana-Casiano, L. Merlivat, L. Barbero-Muñoz, and E. V. Dafner (2005), Fluxes of CO_2 between the atmosphere and the ocean during the POMME project in the northeast Atlantic Ocean during 2001, *J. Geophys. Res.*, *110*, C07S11, doi:10.1029/2004JC002763.

González-Dávila, M., J. M. Santana-Casiano, and E. F. González-Dávila (2007), Interannual variability of the upper ocean carbon cycle in the northeast Atlantic Ocean, *Geophys. Res. Lett.*, *34*, L07608, doi:10.1029/2006GL028145.

Hendricks, M. B., M. L. Bender, and B. A. Barnett (2004), Net and gross O_2 production in the southern ocean from measurements of biological O_2 saturation and its triple isotope composition, *Deep Sea Res. Part I*, *51*, 1541–1561.

Hood, M. E., and L. Merlivat (2001), Annual to interannual variations of fCO_2 in the northwestern Mediterranean Sea: Results from hourly measurements made by CARIOCA buoys, 1995–1997, *J. Mar. Res.*, *59*, 113–131.

Johnson, K. S., L. J. Coletti, and F. P. Chavez (2006), Diel nitrate cycles observed with in situ sensors predict monthly and annual new production, *Deep Sea Res. Part I*, *53*, 561–573.

Josse, P., G. Caniaux, and S. et Planton (1996), Introduction du mélange diapycnal dans un modèle 1D de couche de mélange océanique, Volume d'actes des Ateliers de Modélisation de l'Atmosphère, CNRM Ed., Toulouse, 3–4 Decembre, pp. 139–143.

Kortzinger, A., W. Koeve, P. Kahler, and L. Mintrop (2001), C:N ratios in the mixed layer during the productive season in the northeast Atlantic Ocean, *Deep Sea Res. Part I*, *48*, 661–688.

Legal, C., P. Klein, A. M. Treguier, and J. Paillet (2007), Diagnosis of the vertical motions in a mesoscale stirring region, *J. Phys. Oceanogr.*, *37*(5), 1413–1424.

Lévy, M., M. Gavart, L. Mémery, G. Caniaux, and A. Paci (2005), A four-dimensional mesoscale map of the spring bloom in the northeast Atlantic (POMME experiment): Results of a prognostic model, *J. Geophys. Res.*, *110*, C07S21, doi:10.1029/2004JC002588.

Lueker, T. J., A. G. Dickson, and C. D. Keeling (2000), Ocean pCO_2 calculated from dissolved inorganic carbon, alkalinity, and equations for K1 and K2: Validation based on laboratory measurements of CO_2 gas and seawater at equilibrium, *Mar. Chem.*, *70*, 105–119.

Marra, J. (2002), Approaches to the measurement of plankton production, in *Phytoplankton Productivity: Carbon Assimilation in Marine and Freshwater Ecosystems*, edited by P. J. le. B. Williams, D. N. Thomas, and C. S. Reynolds, pp. 78–108, Blackwell, Malden, Mass.

Mémery, L., G. Reverdin, J. Paillet, and A. Oschlies (2005), Introduction to the POMME special section: Thermocline ventilation and biogeochemical tracer distribution in the northeast Atlantic Ocean and impact of mesoscale dynamics, *J. Geophys. Res.*, *110*, C07S01, doi:10.1029/2005JC002976.

Merlivat, L., and P. Brault (1995), CARIOCA buoy: Carbon dioxide monitor, *Sea Technol.*, *10*, 23–30.

Paci, A., G. Caniaux, M. Gavart, H. Giordani, M. Lévy, L. Prieur, and G. Reverdin (2005), A high-resolution simulation of the ocean during the POMME experiment: Simulation results and comparison with observations, *J. Geophys. Res.*, *110*, C07S09, doi:10.1029/2004JC002712.

Paci, A., G. Caniaux, H. Giordani, M. Lévy, L. Prieur, and G. Reverdin (2007), A high-resolution simulation of the ocean during the POMME experiment: Mesoscale variability and near surface processes, *J. Geophys. Res.*, *112*, C04007, doi:10.1029/2005JC003389.

Paillet, J., and M. Arhan (1996), Shallow pycnoclines and mode waters subduction in the eastern North Atlantic, *J. Phys. Oceanogr.*, *26*, 96–114.

Pérez, F. F., M. Alvarez, and A. F. Ríos (2002), Improvements of the back-calculation technique for estimating anthropogenic CO_2, *Deep Sea Res. Part I*, *49*, 859–875.

Resplandy, L., M. Lévy, F. D'Ovidio, and L. Merlivat (2009), Impact of sub-mesoscale variability in estimating the air-sea CO_2 exchange: Results from a model study of the POMME experiment, *Global Biogeochem. Cycles*, doi:10.1029/2008GB003239, in press.

Robinson, C., P. Serret, G. Tilstone, E. Teira, M. V. Zunkov, A. P. Rees, and E. M. S. Woodward (2002), Plankton respiration in the Eastern Atlantic Ocean, *Deep Sea Res. Part I*, *49*, 787–813.

Sabine, C., et al. (2004), The oceanic sink for anthropogenic CO_2, *Science*, *305*(5682), 367–371, doi:10.1126/science.1097403.

Takahashi, T., et al. (2007), Climatological mean and decadal changes in surface ocean pCO_2, and net sea-air CO_2 flux over the global oceans, paper presented at the UNESCO Meeting, Paris, France, 11–14 April.

Wanninkhof, R. (1992), Relationship between wind speed and gas exchange over the ocean, *J. Geophys. Res.*, *97*, 7373–7382.

Weiss, R. F. (1974), Carbon dioxide in water and seawater: The solubility of a non-ideal gas, *Mar. Chem.*, *2*, 203–215.

Zeebe, R., and D. Wolf-Gladrow (2001), *CO_2 in Seawater: Equilibrium, Kinetics, Isotopes*, *Elsevier Oceanogr. Ser.*, 65 pp., Elsevier, New York.

J. Boutin, L. Merlivat, and G. Reverdin, Laboratoire d'Océanographie et du Climat-Expérimentation et Approches Numériques (ex LODYC)/IPSL, Centre National de la Recherche Scientifique, Université Pierre et Marie Curie, 4 place Jussieu, F-75252 Paris, France. (merlivat@locean-ipsl.upmc.fr)

G. Caniaux, Centre National de Recherches Meteorologiques/GAME (Météo-France/CNRS), 42 Avenue Gaspard Coriolis, 31057 Toulouse, France.

M. Gonzalez Davila, Facultad de Ciencias del Mar, Universidad de Las Palmas de Gran Canaria, Campus Universitario de Tafira, 35017 Las Palmas, Spain.